Polar vs. apolar alignment in systems of polar self-propelled particles

2011 J. Phys.: Conf. Ser. 297 012014

(http://iopscience.iop.org/1742-6596/297/1/012014)

Journal of Physics: Conference Series **297** (2011) 012014 doi:10.1088/1742-6596/297/1/012014

Polar vs. apolar alignment in systems of polar self-propelled particles

Fernando Peruani
Max Planck for the Physics of Complex Systems, Nöthnitzer str. 38, Dresden, Germany

Francesco Ginelli
Service de Physique de l'Etat Condensé, CEA-Saclay, 91191 Gif-sur-Yvette, France

Markus Bär
Physikalisch-Technische Bundesanstalt, Abbestrasse 2-12, 10587 Berlin, Germany

Hugues Chaté
Service de Physique de l'Etat Condensé, CEA-Saclay, 91191 Gif-sur-Yvette, France

Abstract. The symmetry of the alignment mechanism in systems of polar self-propelled particles determines the possible macroscopic large-scale patterns that can emerge. Here we compare polar and apolar alignment. These systems share some common features like giant number fluctuations in the ordered phase and self-segregation in the form of bands near the onset of orientational order. Despite these similarities, there are essential differences like the symmetry of the ordered phase and the stability of the bands.

1. Introduction

Systems of collectively moving entities are ubiquitous in nature, ranging from flocks of birds [1, 2, 3], insect swarms [5, 6], bacterial collective motion [7, 8], to even driven granular media [9, 10, 11, 14]. Beyond the complexity of each system, it is possible to classify the interaction among the moving entities according to its symmetry, which can be either polar or apolar. Polar (or ferromagnetic) interactions lead to parallel alignment of the velocity of the moving objects, while apolar (or nematic) interactions allow both, parallel as well as antiparallel alignment. Fish, birds, and insects seem to exhibit polar alignment [1, 2, 3, 5, 6]. Bacteria and driven granular media often display apolar alignment [8, 9, 10, 11]. The physical origin of the alignment mechanism varies among these examples and it is difficult to identify a particular physical interaction with a given symmetry in these non-equilibrium systems. For instance, steric interactions among elongated self-propelled objects lead to apolar alignment. This can be easily observed in realistic self-propelled rod models [12], experiments with driven rods [10, 11], and experiments with gliding bacteria [8]. However, if the objects are isotropic, volume exclusion effects can result in a polar alignment, as observed in models [13] and experiments [14] with polarly driven disks.

Here we focus on the collective large-scale patterns emerging in systems of point particles moving in two-dimensions at constant speed. We compare the dynamics and macroscopic properties of self-propelled particles interacting by a polar and an apolar velocity alignment mechanism. We list the common features and highlight the differences. We provide in this way a summary of the two main classes of polar self-propelled particle systems.

2. Equation of motion of self-propelled particles

The evolution of the i-th particle is given by the following updating rules:

$$\mathbf{x}_i^{t+\Delta t} = \mathbf{x}_i^t + v_0 e^{\mathrm{i}\,\theta_i^t}\Delta t \tag{1}$$

$$\theta_i^{t+\Delta t} = \arg\left(\sum_{|\mathbf{x}_i^t-\mathbf{x}_j^t|\le\epsilon} f\left(\theta_j^t,\theta_i^t\right) e^{\mathrm{i}\,\theta_j^t}\right) + \eta_i^t \tag{2}$$

where $\mathbf{x}_i^t$ is the position of the particle and θ_i^t its direction of motion at time t, v_0 the active particle speed, $\arg(\mathbf{b})$ indicates the argument of the imaginary number $\mathbf{b}$, η_i^t is a delta-correlated white noise of strength η [15], and Δt is the temporal time step. Notice that Eqs. (1) and (2) can be considered the limiting case of very fast angular relaxation of a system of equations of the form:

$$\dot{\mathbf{x}}_i = v_0 e^{\mathrm{i}\,\theta_i}\,, \quad \dot{\theta}_i = -\gamma\frac{\partial U}{\partial\theta_i}(\mathbf{x_i},\theta_i) + \tilde{\eta}_i(t)\,,$$

as discussed in [16]. The symmetry of the alignment mechanism is contained in the function f which is defined as:

$$f\left(\theta_j^t,\theta_i^t\right) = \begin{cases} 1 & \text{for polar alignment} \\ \mathrm{sign}\left(\cos(\theta_j^t-\theta_i^t)\right) & \text{for apolar alignment} \end{cases}, \tag{3}$$

where $\mathrm{sign}(x)$ return a $+1$ if $x \ge 0$ and -1 otherwise. Eqs. (1) and (2) together with Eq. (3) defined the so-called Vicsek model [17, 18] for polar alignment, and the model for (ideal) self-propelled rods introduced in [16, 19] for apolar alignment.

2.1. Order parameters

The orientational order can be characterized by the following order parameters. The polar (ferromagnetic) order parameter is defined by:

$$\phi = \left\langle\left|\frac{1}{N}\sum_{k=1}^{N}\exp(\mathrm{i}\,\theta_k^t)\right|\right\rangle, \tag{4}$$

where $\langle\ldots\rangle$ denotes time-average and N stands for the total number of particles in the system. ϕ takes the value 1 when all particles move in the same direction, while in the disordered phase, i.e., when particles move in any direction with equal probability, it vanishes. On the other hand, the apolar (nematic) ordered parameter takes the form:

$$S = \left\langle\left|\frac{1}{N}\sum_{k=1}^{N}\exp(\mathrm{i}\,2\,\theta_k^t)\right|\right\rangle. \tag{5}$$

Formally, S can be derived from the order parameter matrix Q of *liquid crystals* (LC) [20], as the largest eigenvalue (which here we have normalized such that $S^{LC} \in [0,1]$). When the system is perfectly nematically ordered, i.e., when particles move in opposite directions along the same axis, S takes the value 1. In summary, a perfectly polarly ordered phase is characterized by $\phi = S = 1$, while for a genuine apolarly ordered phase, $\phi = 0$ and $S = 1$.

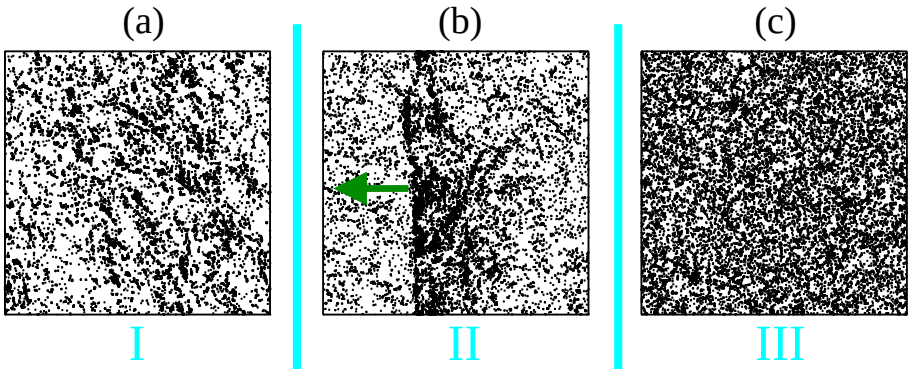

Figure 1. Typical steady-state snapshots for SPPs with polar alignment at different noise values (linear size $L = 512$, particle density $\rho = 1/8$, active speed $v_0 = 1/4$). The snapshots correspond to phase I, (a) $\eta = 0.06$, phase II, (b) $\eta = 0.1$, and phase III, (c) $\eta = 0.19$. The arrow in (b) indicates the direction of motion of the high-density band.

.

3. Macroscopic patterns with polar alignment

We start out by reviewing the large-scale properties of SPPs with polar alignment. If we fix the active speed v_0 and the density ρ, while varying the noise strength η we observe the emergence of three statistically distinct stationary states or phases. Two of these phases correspond to orientationally ordered phases, while the third one is a disordered phase. We refer to these phases as phase I, II, and III by increasing value of η.

Phase I exhibits polar long-range order and is characterized by the absence of regular large-scale, high density structures, see Fig.1(a). Due to this fact, it is often said that this phase is spatially homogeneous albeit with large density fluctuations. The presence of polar long-range order implies that $\phi(\eta) \to K_0(\eta)$ as the system size $L \to \infty$, with $K_0(\eta) > 0$ a constant that depends only on η. Phase I also exhibits giant number fluctuations (NF). NF are defined as $\Delta n^2(\ell) = \langle (n(\ell) - \langle n \rangle(\ell))^2 \rangle$, where $n(\ell)$ stands for the number of particles in a box of linear size ℓ. The average number of particles is $\langle n \rangle = \rho \ell^2$ while $\Delta n(\ell)$ is expected to be $\Delta n \propto \langle n \rangle^\alpha$. Giant NF correspond to $\alpha > \frac{1}{2}$ [21]. In [18] it was shown that $\alpha \sim 0.8$ for phase I.

By increasing η we reach a point at which large-scale, elongated, high-density, high-order solitary structures emerge. These structures, that we refer to as bands, move at roughly constant speed, see Fig.1(b). A system of SPPs with polar alignment can display multiple bands. The low-density region in between bands is disordered and there is no characteristic separation length between bands [18]. In summary, phase II is characterized by polar long-range order and the presence of traveling bands. If η is increased further, we reach phase III that exhibits local and global disorder, see Fig.1(c).

4. Macroscopic patterns with apolar alignment

Now we focus on a system of SPPs with apolar alignment. While sweeping η, keeping the active speed and the density fixed, we observe the emergence of four statistically distinct stationary states or phases, see Figs. 3-4. Two of these four regimes correspond to ordered phases while the other two to disordered phases. At the two extremes, very high and very low values of η, the system is spatially homogeneous, Figs. 3(a,e). At intermediate values of η, spontaneous density segregation occurs in the form of a high-density ordered region along which the particles move back and forth, Figs. 3(b-d). It is important to stress that macroscopic polar order always remains near zero. Nevertheless, if we look at very short length scales, we observe that the

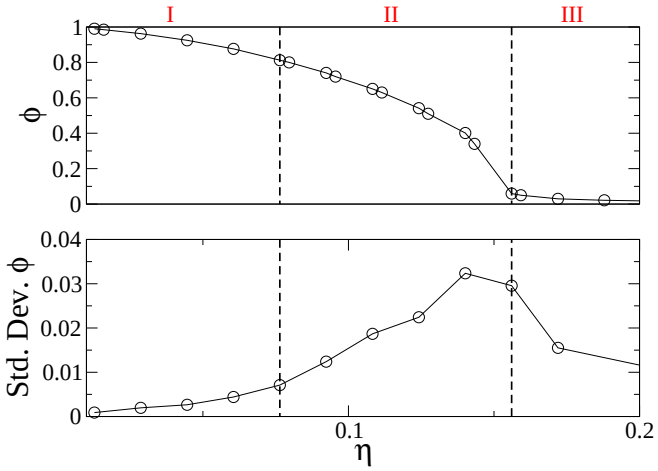

Figure 2. Polar order parameter ϕ and its standard deviation as function of the noise amplitude η (other parameters as in Fig. 1).

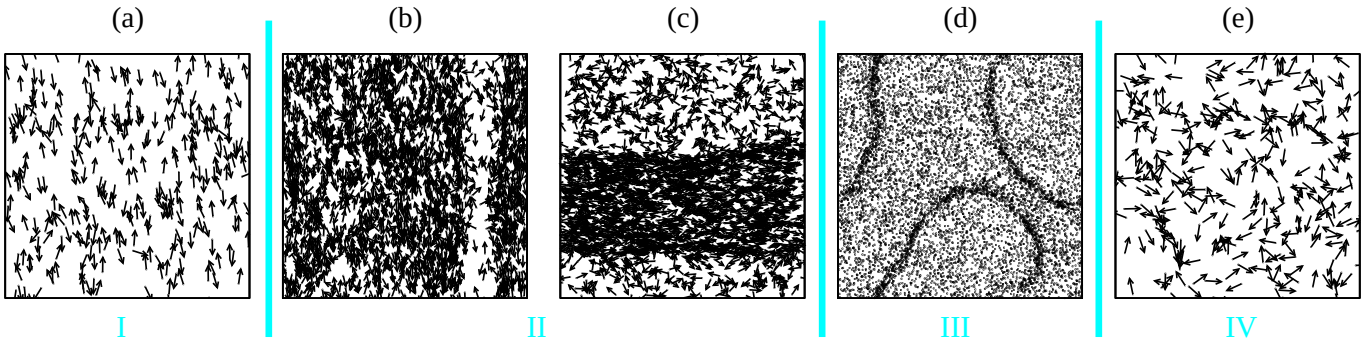

Figure 3. Typical steady-state snapshots for SPPs with apolar alignment at different noise values (linear size $L = 2048$, density $\rho = 1/8$, and velocity $v_0 = 1/2$). (a) $\eta = 0.08$, (b) $\eta = 0.10$, (c) $\eta = 0.13$, (d) $\eta = 0.168$, (e) $\eta = 0.20$. Arrows indicate the polar orientation of particles (except in (d)); only a fraction of the particles are shown for clarity reasons.

apolar ordered phase is formed by polarly oriented clusters. In the following we provide a more quantitative description of these four phases, which we name, by increasing value of η, phase I to IV. Phase I exhibits true long-range apolar (nematic) order and is spatially homogeneous. This apolar order corresponds to two subpopulations of particles of roughly equal size that migrate in opposite directions (Fig. 5a). We conclude that the apolar order is truly long-range by looking at scaling of the apolar order parameter S with the system size. From Fig. 5a, it seems that $S(L)$ approaches a constant asymptotic value $C_0(\eta)$ for $L \to \infty$, with $C_0(\eta) > 0$, indicating the possible existence of true long-range apolar order. Another remarkable feature of phase I is the presence of giant number fluctuations (NF). Fig. 5b shows the scaling $\Delta n \propto \langle n \rangle^{\alpha}$ in phase I, where it is found again that $\alpha \sim 0.8$.

By increasing η we move from phase I to phase II. Its onset is characterized by the emergence of a narrow, low-density, disordered channel. This channel becomes wider at larger η values, so that one can speak of a high-density ordered region along which particles travel in both directions. The high-density region exhibits apolar order with properties similar to those

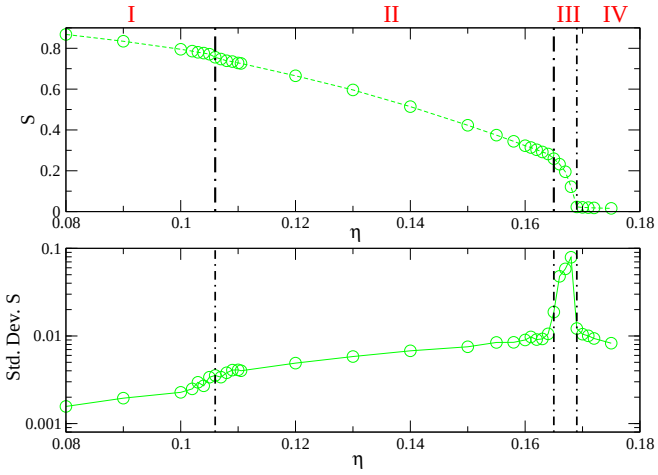

Figure 4. Apolar (nematic) order parameter S and its standard deviation as function of the noise amplitude η (other parameters as in Fig. 3).

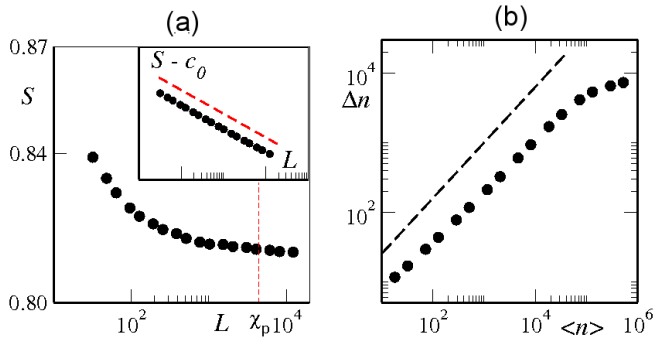

Figure 5. Phase I of SPPs with apolar alignment: long-range apolar order and giant number fluctuations ($\rho = 1/8$, $v_0 = 1/2$, and $\eta = 0.095$). (a) Apolar order parameter S vs system size L in square domains. The vertical red dashed line marks the persistence length $\chi \approx 4400$ that particles can travel before performing a U-turn. Inset: $S - C_0 = 0.813063$ vs L (red dashed line: $L^{-2/3}$ decay). (b) Number fluctuations Δn as function of $\langle n \rangle$. The dashed line correspond to an algebraic growth with exponent 0.8 (simulations with $L = 4096$). See Ref. [19].

observed in phase I: true long-range order and giant NF. The (rescaled) region possesses a well-defined profile with sharper and sharper edges as L increases (Fig. 6a). The fraction area Ω occupied by the dense region is thus asymptotically independent of system size, and it decreases continuously as the noise strength η increases (Fig. 6b).

By increasing η even further, we reach phase III, where the dense region becomes unstable and constantly bend, merge, break and reform. As result of this dynamics, $S(t)$ fluctuates strongly and on very large time scales, but its average decreases as $1/\sqrt{N}$ [19]. Thus, phase III is characterized by the absence of long-range order and the presence of large correlation lengths and times. At even larger η values, we find phase IV, which exhibits local and global disorder on small length- and time-scales, and is spatially homogeneous.

It is difficult to accurately locate the three boundaries that separate the four phases. Fig. 7 is the result of an important numerical effort and shows a reliable estimate of $\eta_c^{I-II}(\rho)$, $\eta_c^{II-III}(\rho)$,

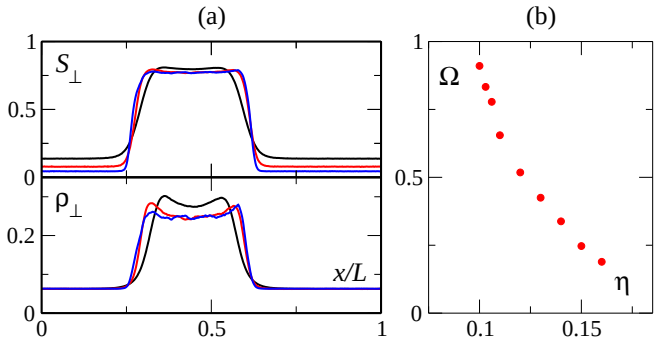

Figure 6. Phase II of SPPs with apolar alignment is characterized by the presence of an elongated high-density, high-order region. (a) The rescaled transverse density (top) and nematic order (bottom) profile in square domains of linear size $L = 512$ (black), 1024 (red), and 2048 (blue) at $\eta = 0.14$ (other parameters as in Fig. 5). (b) Surface fraction Ω occupied by the band as a function of noise amplitude η. See Ref. [19].

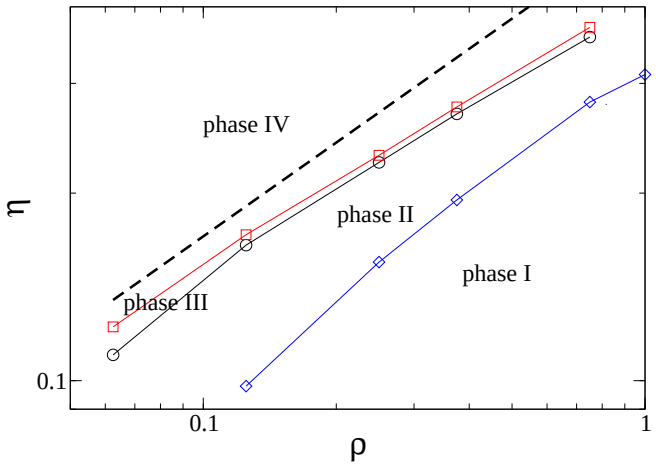

Figure 7. Phase diagram - Critical value of η, separating the four phases, as function of the density. Thresholds obtained for systems of size $L = 1024$ and $v_0 = 1/2$. The dashed line corresponds to the scaling $\eta \propto \rho^{1/2}$.

and $\eta_c^{III-IV}(\rho)$. We are interested in the scaling of $\eta_c^{A-B}(\rho) \propto \rho^{\gamma_{A-B}}$, where $A - B$ refers to some of the three boundaries. Assuming an homogeneous distribution of particles, we can expect $\eta_c^{A-B}(\rho)$ to be proportional to the inverse of the mean free path, i.e., $\propto \rho^{1/2}$. This argument would apply particularly to $\eta_c^{III-IV}(\rho)$. Moreover, for SPPs with polar alignment, this seems to be the case, i.e., $\eta_c^{II-III}(\rho) \propto \rho^{1/2}$, see Fig. 1 and [18]. However, for SPPs with apolar alignment this scaling only seems to hold for $\eta_c^{IV-III}(\rho)$ at very low density. At high density, $\eta_c^{IV-III}(\rho)$ is characterized by $\gamma_{IV-III} \sim 0.43$, suggesting the existence of a more complex mechanism regulating the self-organization of the SPPs particles. Fig. 7 also shows that the parameter range at which phase III is observed shrinks as the density is increased. This finding suggests that at higher densities phase III may not exist. Finally, we notice that $\eta_c^{I-II}(\rho)$ behaves differently than a power-law. Currently, we lack a theoretical understanding of these intriguing numerical results.

5. Comparison between polar and apolar alignment

Self-propelled particles moving at constant speed with either polar or apolar alignment exhibit a phase transition from a disordered to orientationally ordered phase. For both alignments the order seems to be long-range, being purely polar for polar alignment and purely apolar (nematic) for apolar alignment. It has been shown theoretically that self-propelled particles with polar alignment can display long-range order [22]. However, the claim about the existence of apolar long-range order is exclusively based on large-scale simulations and a theoretical justification is still missing. Assuming that the findings here reported for large-scale simulations hold in the thermodynamical limit, we conclude that SPPs with polar alignment exhibit three phases, while with apolar alignment, the phases are four. For both alignments, there are two ordered phases, one of them spatially "homogeneous", though with giant number fluctuations with roughly the same critical exponent 0.8, while the other one is characterized by the presence of high-density, high ordered regions. For polar alignment, the system can display multiple solitary bands. These bands are traveling bands whose moving direction is perpendicular to the long axis of the band, i.e., particles are aligned roughly in the same direction exhibited by the band velocity. On the other hand, for apolar alignment, we observe only one dense region. This region does not move and is composed of two populations of particles moving in opposite direction along its axis. For polar alignment there is one disordered phase characterized by local and global disorder. SPPs with apolar alignment also exhibit a similar phase, however these particles also display an intriguing disordered phase where particle self-segregation in the form of highly dynamical bands occur.

Bands in phase II, for both, SPPs with polar as well as with apolar alignment, are strongly influenced by the implemented boundary conditions. More specifically, bands tend to be parallel to the size of the simulation box. It has been suggested in [26] that bands in SPPs with polar alignment may be a finite size effect that becomes particularly evident at high velocity values. Here, we have shown that these bands also emerge at low density and low velocity values. Moreover, transient bands are also observed in simulations using reflecting boundary conditions (data not shown), and even in lattice-gas simulations [28]. In summary, we believe that bands in SPPs with either polar or apolar alignment are a robust property of these systems, provided - and this is the key point - the (linear) system size is larger than a critical L^* value (see discussion in [18]). Nevertheless, we admit that our arguments are just based on numerical evidence and a solid theoretical justification is still lacking. Results by Bertin et al. [25] seem to provide the first theoretical justification of the existence of such bands. To learn about this controversy, see [26, 18, 27, 25]. On the other hand, bands in phase III of SPPs with apolar alignment do not exhibit any influence from the boundary condition, making their existence easier to justify.

Adopting our view, in a coarse-grained description of these systems, the homogeneous disordered phase should get unstable by the emergence of soliton-like structures: traveling bands, for polar alignment, while for apolar alignment, local alignment has to lead to the formation of dynamic bands. In the case of apolar alignment, the onset of global order is not associated to the instability of the disorder homogeneous state, as for polar alignment, but with the stability of the high-density, dynamic band of phase III (Fig. 3d). On the other extreme, well in the "homogeneous" ordered phase, i.e. in phase I of both systems, we can approximate the behavior of the order parameter ϕ and S as:

$$\phi = \frac{2}{\eta}\sin(\eta/2) \tag{6}$$

$$S = \frac{1}{\eta^2}\sin^2(\eta)\,, \tag{7}$$

using a simple mean-field argument as discussed in [23]. From this we can presume that for a given set of parameters v_0, ρ, and η, $\phi(v_0,\rho,\eta) \geq S(v_0,\rho,\eta)$. Moreover, a simple mean-field

analysis of the"homogeneous" disordered phase reveals that, for fixed v_0 and ρ, this phase looses its stability at lower values of η for apolar alignment than for polar alignment [16]. From all this, we learn that is easier to achieve orientational order with polar than with apolar alignment. This comparison also suggests that polar order is more robust than apolar order.

Beyond this rough comparison between both alignment, a theoretical understanding of phase separation that occurs in both systems in the form of high-density, high-order bands is still lacking. For polar alignment, there are some promising recent theoretical results [24, 25] that provide an interesting perspective to this puzzling issue. We hope that in the near future all these open problems will be fully understood.

References

[1] Parrish J K and Hamner W M 1997, *Three Dimensional Animals Groups*, (Cambridge: Cambridge University Press)
[2] Cavagna A et al. 2010 *Proc. Natl. Acad. Sci.* **107** 11865
[3] Bhattacharya K and Vicsek T 2010 *New J. Phys.* **12** 093019
[4] Helbing D, Farkas I, and Vicsek T 2000 *Nature (London)* **407** 487
[5] Buhl J et al. 2006 *Science* **312** 1402
[6] Romanczkuk P, Couzin I D, and L. Schimansky-Geier L 2009 *Phy. Rev. Lett.* **102** 010602 .
[7] Zhang H P et al. 2010 *Proc. Natl. Acad. Sci.* **107** 13626
[8] Peruani F et al. 2011 *unpublished*
[9] Narayan V, Ramaswamy S, and Menon N 2007 *Science* **317** 105
[10] Kudrolli A, Lumay G, Volfson D, and Tsimring L S 2008 *Phys. Rev. Lett.* **100** 058001
[11] Kudrolli A 2010 *Phys. Rev. Lett.* **104** 088001
[12] Peruani F, Deutsch A, and Bär M 2006 *Phys. Rev. E* **74** 030904
[13] Grossman D, Aranson I S, and Ben Jacob E 2008 *New J. Phys.* **10** 023036
[14] Deseigne J, Dauchot O, and Chaté H 2010 *Phys. Rev. Lett.* **105** 098001
[15] The parameter η, given in all figures, is defined as half the width of the noise, which is top-hat distributed and centered around 0. The parameter η is measured in *units* of $\pi/2$, so that $\eta = \delta$ means that $\eta_i^t \in [-\pi\delta/2, \pi\delta/2]$.
[16] Peruani F, Deutsch A, and Bär M 2008 *Eur. Phys. J. Special Topics* **157** 111
[17] Vicsek T, Czirok A, Ben-Jacob E, Cohen I, and Shochet O 1995 *Phys. Rev. Lett.* **75** 1226
[18] Chaté H, Ginelli F, Grégoire G, and Raynaud F 2008 *Phys. Rev. E* **77** 046113
[19] Ginelli F, Peruani F, Bär M, and Chaté H 2010 *Phys. Rev. Lett.* **104** 184502
[20] Doi M and Edwards S F 1986, *The Theory of Polymer Dynamic* (Oxford: Clarendon Press).
[21] Ramaswamy S, Simha R A and Toner J 2003 *Europhys.Lett.* **62**, 196
[22] Toner J and Tu Y 1995 *Phys. Rev. E* **58** 4828; 1995 *Phys. Rev. Lett.* **75** 4326
[23] Peruani F, Schimansky-Geier L, and Bär M 2010 *Eur. Phys. J. Special Topics* **191** 173
[24] Mishra S, Baskaran A, and Marchetti M C 2010 *Phys. Rev. E* **81** 061916
[25] Bertin E, Droz M, and Grégoire G 2006 *Phys. Rev. E* **74** 022101 (2006); 2009 *J. Phys. A* **42** 445001
[26] Nagy M, Daruka I, and Vicsek T 2007 *Physica A* **373** 445
[27] Baglietto G and Albano E 2009 *Phys. Rev. E* **80** 050103
[28] Schaller V et al. 2010 *Nature* **467** 73